Ligand-Induced Chirality in Novel 2D Tin Iodide Perovskite Cl-MBA$_2$SnI$_4$

Clarissa Coccia,[a] Marta Morana,[b] Arup Mahata,*[c,d] Waldemar Kaiser,[c] Marco Moroni,[a] Benedetta Albini,[e] Pietro Galinetto,[e] Chiara Milanese,[a] Alessio Porta,[a] Edoardo Mosconi,[c] Filippo De Angelis,[c,f,g] and Lorenzo Malavasi*[a]

[a] Miss Clarissa, Coccia, Dr. Marco Moroni, Prof. Chiara Milanese, Prof. Alessio Porta, Prof. Lorenzo Malavasi,
Department of Chemistry, University of Pavia, Via Tarameli 12, Pavia 27100, Italy, E-mail: lorenzo.malavasi@unipv.it

[b] Dr. Marta Morana, Department of Earth Science, University of Firenze, Via G. La Pira 4, Firenze 50121, Italy

[c] Dr. Arup Mahata, Dr. Waldemar Kaiser, Dr. Edoardo Mosconi, Prof. Filippo De Angelis, Computational Laboratory for Hybrid/Organic Photovoltaics (CLHYO), Istituto CNR di Scienze e Tecnologie Chimiche "Giulio Natta" (CNR-SCITEC), Perugia 06123, Italy, arup@chy.iith.ac.in

[d]   Dr. Arup Mahata, Department of Chemistry, Indian Institute of Technology Hyderabad, Kandi, Sangareddy, Telangana 502285, India

[e] Dr. Bendetta Albini, Prof. Pietro Galinetto, Department of Physics, University of Pavia, Via Bassi 6, Pavia 27100, Italy

[f] Prof. Filippo De Angelis. Department of Chemistry, Biology and Biotechnology, University of Perugia and INSTM, Perugia 06123, Italy

[g] Prof. Filippo De Angelis. SKKU Institute of Energy Science and Technology (SIEST) Sungkyunkwan University, Suwon, Korea 440-746.

Abstract: Chiral perovskites possess a huge applicative potential in several areas of optoelectronics and spintronics. The development of novel lead-free perovskites with tunable properties is a key topic of current research. Herein, we report a novel lead-free chiral perovskite, namely (R/S-)ClMBA$_2$SnI$_4$ and the corresponding racemic system. The reported ClMBA$_2$SnI$_4$ samples exhibit a low band gap (2.12 eV) together with broad emission extending in the red region of the spectrum (~1.7 eV). Chirality transfer from the organic ligand induces chiroptical activity in the 465-530 nm range. Density function theory calculations show a Rashba type band splitting for the chiral samples and no band splitting for the racemic isomer. Self-trapped exciton formation is origin of the large Stokes shift in the emission. Careful correlation with analogous lead and lead-free chiral perovskites confirms the role of the symmetry-breaking distortions in the inorganic layers associated with the ligands as the source of the observed chiroptical properties providing also preliminary structure-property correlation in 2D chiral perovskites.

Chiral metal halide perovskites (MHPs) are emerging as one of the most appealing classes of chiral materials due to their potential use for chiroptoelectronics, spintronics, and ferroelectrics.[1–4] One of the most common strategies used to induce chirality-dependent properties in MHPs, such as circular dichroism (CD), circular polarized luminescence (CPL), chiro-induced spin selectivity (CISS) effect and ferroelectricity, is based on the introduction of a chiral ligand in low-dimensional MHPs. This approach, coupled with their rich structural tunability, made the preparation of 2D, 1D, and 0D chiral MHPs possible.

Most of the chiral perovskites reported so far are based on the few available chiral ligands on the market such as methylbenzylammonium (MBA), β- methylphenethylammonium (MPEA), 1-(naphthyl)ethylammonium (NEA), R-3- aminopiperidine (3APD), 3-ammonioquinuclidinium (3AQ), and 2- octylamine (2OA).[5–18] In terms of structural motifs, 2D chiral perovskites are those most commonly reported together with 1D systems, while 3D systems have been predicted but not yet realized.[16,19] This directly correlates to the fact that a chiral center requires organic ligands that are too big to be accommodated into a 3D lattice of interconnected octahedra but are easily inserted in layered systems. In terms of metal ion lead, analogously to MHPs for photovoltaics, lead has been used to prepare the vast majority of chiral perovskites, with copper being the second most common metal found in currently available chiral perovskites and with just one Sn-containing system reported to date.[1,2,20–25] Considering the toxicity of lead, it is of significant interest to move towards lead-free systems, as it is happening for photovoltaic applications, particularly in a relatively young field of research as the one of chiral perovskites.

Tin replacement for lead in MHPs is a pervasive strategy not only to provide less toxic materials but also to reduce the band gap towards the optimum according to the Shockley–Queisser limit.[26,27] In addition, tin-based perovskites have similar or superior electronic and optical properties to lead-containing systems, such as higher charge carrier mobilities and long-lived hot carriers.[28] In the field of chiral perovskites, except for the (R-/S-MBA)$_2$SnI$_4$ system (MBA= methylbenzylammonium), no other tin-based materials have been reported so far. However, in view of potential future applications in chiral optoelectronic devices, the use of tin could guarantee a reduced environmental impact and provide the degree of optical properties tunability required. In addition, the design of novel chiral perovskites should be based on solid structure-property correlations, which are the basis of the actual engineering of perovskites for optoelectronic applications. There are only few structure-property correlations works on chiral perovskite, mainly as a consequence of the limited number of phases with solved crystal structures reported, and few rational series of materials where, for example, the impact of organic ligand, central atom, or halide has been progressively and rationally changed to

unveil the respective roles on the chiro-optical response. This is even more dramatic when considering tin-based perovskites.

The performance of chiral perovskites is usually estimated by taking into account the anisotropy factor, g_{CD}, which is the CD normalized to absorption, and it is generally recognized as a quantitative figure-of-merit of chiro-optical activity. In general, higher values of the g_{CD} correlates to higher levels of spin polarizations which are achieved in chiral perovskites without applying an external field. It is imperative to widen the number of available chiral perovskites, particularly lead-free systems, to design MHPs with enhanced anisotropy factor and identify relevant compositional and structural parameters.

With this aim, we designed the $ClMBA_2SnI_4$ chiral perovskites (ClMBA = 1-(4-chlorophenyl)ethanamine) and investigated its crystal structure by room temperature single-crystal x-ray diffraction (SCXRD) together with optical spectroscopy and computational modelling. Single crystals of the *R*/*S*- enantiomers and racemic (*rac*) form of $ClMBA_2SnI_4$ have been prepared by solution chemistry (see Supporting Information, SI) and the respective crystal structures are solved by SCXRD. The crystallographic data and selected structural parameters are reported in Table 1. Figure 1 reports a sketch of the respective structures and the appearance of the red crystals of (*R*-$ClMBA)_2SnI_4$.

Table 1. Crystal structure data for (*R*- $ClMBA)_2SnI_4$, (*S*- $ClMBA)_2SnI_4$, and (*rac*-$ClMBA)_2SnI_4$.

	(*R*-ClMBA)$_2$SnI$_4$	(*S*-ClMBA)$_2$SnI$_4$	(*rac*-ClMBA)$_2$SnI$_4$
Empirical formula	$C_{16}H_{22}N_2Cl_2I_4Sn$	$C_{16}H_{22}N_2Cl_2I_4Sn$	$C_{16}H_{22}N_2Cl_2I_4Sn$
Formula weight	939.54	939.54	939.54
Temperature	273.5 K	273.5 K	273.5 K
Wavelength	0.71073	0.71073	0.71073
Crystal system	Triclinic	Triclinic	Orthorhombic
Space group	*P1*	*P1*	*Pnma*
Lattice parameters	a = 8.9234(6) Å	a = 8.9085(15) Å	a = = 8.6242(5) Å
	b = 9.0822(8) Å	b = 9.0993(16) Å	b = 9.2932(4) Å
	c = 16.2963(13) Å	c = 16.295(3) Å	c = 32.1932(17) Å

Volume	1306.33(18) Å^3	1306.3(4) Å^3	2580.2(2) Å^3
Z	2	2	4
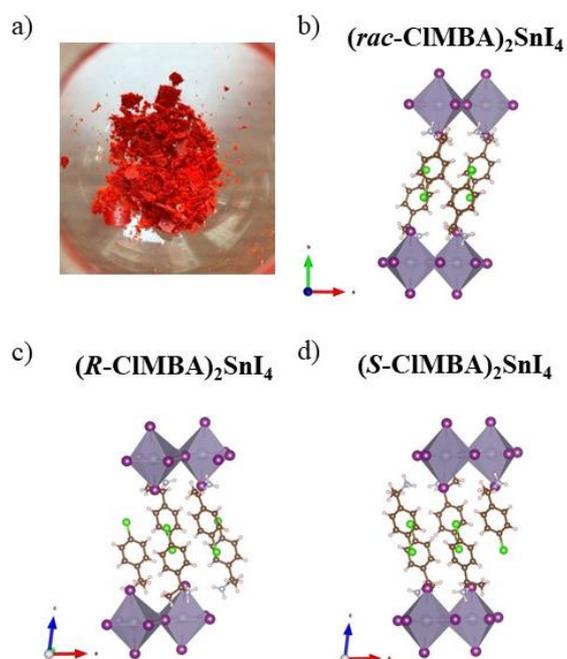
Figure 1. a) Appearance of the crystal of (R-ClMBA)$_2$SnI$_4$; sketch of the crystal structures of (*rac*-ClMBA)$_2$SnI$_4$ (b), (R-ClMBA)$_2$SnI$_4$ (c), and (S-ClMBA)$_2$SnI$_4$ (d).

The structural arrangement is typical of 2D perovskites with a slab of corner-sharing octahedra separated by two molecules of the ClMBA ligand. The two chiral compositions, *i.e.* (R-ClMBA)$_2$SnI$_4$ and (S-ClMBA)$_2$SnI$_4$, crystallize into the triclinic *P*1 chiral space group, while the racemic form in the centro-symmetric orthorhombic *Pnma*. ClMBA ligand introduces a further reduction of symmetry compared to MBA, where the chiral (R-MBA)$_2$SnI$_4$ and (S-MBA)$_2$SnI$_4$ crystallize in the orthorhombic *P*2$_1$2$_1$2$_1$ space group.[25]

The octahedra of (R-ClMBA)$_2$SnI$_4$ and (S-ClMBA)$_2$SnI$_4$ are distorted, presenting six different bond lengths and an in-plane Sn-I-Sn angle significantly lower than the ideal value of 180° (around 155°). Such effects are closely related to the hydrogen bond formation and the penetration of the protonated amine group.[25,29,30] The level of octahedral distortion has been quantified in terms of the octahedral quadratic elongation (λ_{oct}), and their bond angle variance (σ_{oct}^2), as defined by Robison *et al.*, as well as by calculating the distortion index, *D*.[31,32] The respective values for these parameters are reported in Table S1 of SI for (R-ClMBA)$_2$SnI$_4$, (S-ClMBA)$_2$SnI$_4$, and (*rac*-ClMBA)$_2$SnI$_4$. While

the quadratic elongation shows a slight difference among the three perovskites, the racemic compound is characterized by a higher value of both the bond angle variance and the distortion index. Together with the data for the actual perovskites, we added in Table S1, SI, the structural parameters for the other Sn-based chiral system known to date, as well as for the Pb analogues $(ClMBA)_2PbI_4$ and $(MBA)_2PbI_4$, to identify possible correlations as a function of central metal and organic ligand. The variation of quadratic elongation *vs*. bond angle variance and of these two parameters as a function of NH_3 penetration is reported in Figure S1, SI. As a general trend, lead-containing systems show smaller values of quadratic elongation and of the distortion index for the same organic cation, and slightly higher values of the bond angle variance. For comparison, the *D* value for (*R*-ClMBA)$_2$SnI$_4$ and (*S*-ClMBA)$_2$SnI$_4$ is about half of that reported by Lu and co-workers for (*R*-MBA)$_2$SnI$_4$ and (*S*-MBA)$_2$SnI$_4$, namely ~0.004 and ~0.008, respectively.[25] On the other hand, by keeping the same central metal (Pb or Sn) and moving from MBA to ClMBA, a general reduction of the distortion index and of the quadratic elongation is observed. However, we realize that the number of chiral 2D perovskites (with solved crystal structure) available and suitable to extract more solid structural correlations is limited. Still, we may, with these preliminary results, suggest a possible route to tune the distortion parameters.

Structural stability of the three 2D perovskites reported here has been determined by means of differential scanning calorimetry (DSC). The respective DSC traces in the range -80-140°C are reported in Figure S2, and do not show any peak indicating the presence of structural phase transitions.

The optical properties of (*R*-ClMBA)$_2$SnI$_4$, (*S*-ClMBA)$_2$SnI$_4$, and (*rac*-ClMBA)$_2$SnI$_4$ have been determined by UV-Vis, micro-photoluminescence (μPL), and circular dichroism spectra. Figure 2a-c shows the corresponding results.
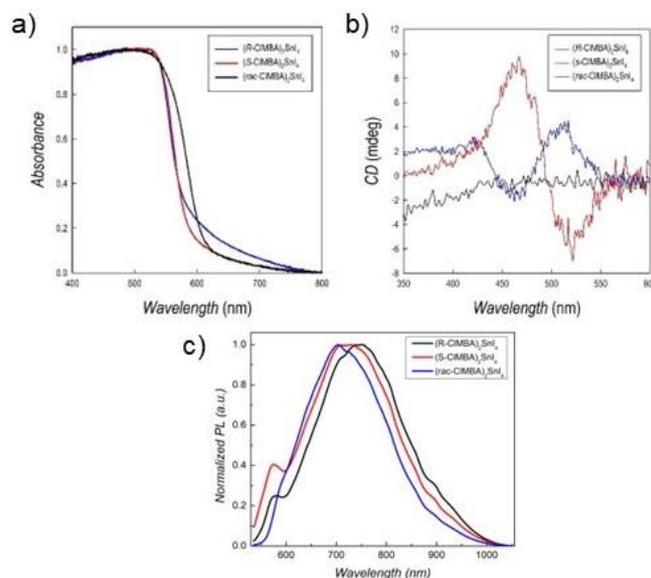
Figure 2. a) Absorbance; b) CD, and c) µPL of (R-ClMBA)$_2$SnI$_4$, (S-ClMBA)$_2$SnI$_4$, and (rac-ClMBA)$_2$SnI$_4$.

Absorption spectra show narrow optical band edges around 600 nm with a slight red-shift for (rac-ClMBA)$_2$SnI$_4$ compared to the two chiral perovskites. The corresponding optical band gap values have been extracted from the Tauc plots for direct transition (Figure S3) and correspond to about 2.12 eV for the two chiral perovskites and 2.08 for the racemic compound. The band gap of the present samples is among the lowest band gap reported so far for a 2D chiral perovskite, being that of lead-containing materials around 2.3-2.8 eV and ~2.55 for the only other tin-based 2D chiral perovskite, namely (R/S-MBA)$_2$SnI$_4$.[1,4,25]

The circular dichroism, carried out on thin films (Figure 2b) of (R/S-ClMBA)$_2$SnI$_4$, presents signals in the 400-550 nm range, while (rac-ClMBA)$_2$SnI$_4$ does not show any CD. The CD spectra of the two chiral materials have opposite peaks at the same wavelengths, *i.e.* ~465 and ~520 nm, with the last one correlating very well with the linear absorption shown in Figure 2a, interpreted as the Cotton effect, indicating that the chiroptical properties arise from the Sn-I inorganic framework (the chiral group has CD signals around 250 nm, see Figure S4).[33,34] From the CD data we calculated the asymmetry factor, g_{CD}, which resulted to be around 1×10^{-4} for both enantiomers, in line with the values usually found in 2D chiral perovskites. This value is close to the value we extracted from ref. 23, where the asymmetry factor is not reported, for (R/S-ClMBA)$_2$SnI$_4$ corresponding to about 3×10^{-4}.

The PL spectra of the three 2D perovskites shown in Figure 2c present broad peaks (FWHM of about 200 nm) with a significant Stokes shift and emission centered around 720-740 nm (1.72-1.67 eV). Such broad emission is not found in the corresponding Pb-containing perovskites where, in

addition, the Stokes shift is of only 15-20 nm.[34] This difference in the emission properties may be related to the degree of distortion of the octahedra. As a matter of fact, by comparing Table S1, it can be seen that the distortion index, as well as the bond-angle variance values of the present samples, is significantly higher than the corresponding Pb-analogues.[29,35–37] We remark that achieving chiral perovskites with emission in the red part of the visible spectrum may be of interest for future applications and the present samples are among the first examples of chiral lead-free 2D perovskites possessing such characteristic.

To gain insight into the electronic structure of the $ClMBA_2SnI_4$ compounds, Density Functional Theory (DFT) calculations have been carried out for the *R*- and *S*- and racemic configurations. As expected, the three enantiomers show very similar electronic properties with the band gap of 2.50, 2.51 and 2.39 eV for the *R*- and *S*- and racemic configurations, respectively, which is consistent with the experimental band gap trend showing a little lower band gap for the racemic isomer compared to the chiral samples. Figure 3a shows the projected densities of states (DOS) with the contributions of different atomic species for the *R*-isomers (see Figure S5 in SI for *S*- and Racemic isomers). As can be seen, the band edges are dominated by I and Sn contributions, while the Cl contributions lies far from the band edges as also evidenced by the band edge wave functions (Figure S6). Further, we have calculated the electronic band structure of the three systems and the results (Figure 3b-c and Figure S7) show that all the structures have a direct band gap, which is consistent with the experimental optical results.

To investigate the spin characteristics, we have calculated the spin splitting of the electronic band structures for chiral and racemic isomers by calculating the Rashba spin–orbit splitting. Typically, a specific conformational characteristic of organic cations with chiral space group can exert inorganic layer distortion in such a way that breaks the inversion symmetry of the system, leading to Rashba spin–orbit splitting. Such spin splitting, in principle, should be absent in racemic isomer due to presence of centro-symmetric space group in the structure. As happens in typical Rashba spin–orbit splitting, both valence and conduction band split away from the Γ point, leading to valence band maximum (VBM) and conduction band minimum (CBM) which are shifted in k-space by Δk, with the band energy splitting ($\varepsilon^{\neq}$).[38–40] The Rashba interaction parameter is defined as $\alpha = \varepsilon^{\neq}/2\Delta k$. The band structure of chiral (R-isomer) and racemic isomers have been shown in Figure 3b-c, whereas the *S*-isomer has been shown in Figure S7. As can be seen from Figure 3b-c, and Table 1, the frontier bands (both VB and CB) show a Rashba type band splitting, with the highest spin splitting values of 17.8 and 16.4 meV for the conduction and valence band, respectively for the *R*-isomer. *S*-isomer also shows almost similar types of splitting values of 16.9 and 18.7 meV for the frontier conduction and valence band, respectively. As expected, no band splitting has been found for the racemic isomer.

While looking at the Rashba parameter, the *R*- and *S*-isomer show the maximum values of 1.06 and 1.03 eV Å, respectively.

Furthermore, we have attempted to find out the underlying reason for the broad emission by investigating the energetics of the self-trapped excitons (STE) emission pathway. For a ready comparison, we have studied our Sn-based (*R*-isomer) system and the corresponding Pb counterpart, where such broad emission is found to be absent.[34] STE emission energy has been calculated, following the approach of our previous studies, by considering the energy difference between the energies of the triplet and singlet states (at the equilibrium geometry of triplet state) as schematically described by point 3 and point 4, respectively in the Figure 3d.[41,42] We have found an excellent agreement of emission energy of 1.70 eV compared to that of experiment, where the emission peak appears around 720-740 nm (1.72-1.67 eV). Furthermore, as shown in Figure 3e, the Kohn-Sham (KS) orbitals of the relaxed excited triplet state shows the different spatial localization of the electron and hole charge density along with substantial Sn-I bond length lengthening (average 3.54 Å) and shortening (average 3.06 Å), thus indicating the formation of STE. On the other hand, the Pb-counterpart shows a delocalized electron and hole charge density as shown in Figure S8 in SI. Furthermore, the calculated triplet and singlet relaxation energies, as depicted in Figure 3d, for the Sn-system are 277 and 565 meV, respectively, compared to that of 88 and 56 meV for Pb-system. Therefore, the broad *vs*. sharp emission in Sn- and Pb-systems can be assigned for localized (STE formation) and delocalized (band-to-band transition) exited states, respectively. It is noteworthy to mention that halide vacancies may also open emission channels, which may contribute to the broad emission. Nevertheless, our high-level calculations provide a vis-à-vis comparison of the excited state behavior of the Sn- and Pb-systems, reasonably explaining the experimental emission characteristics.
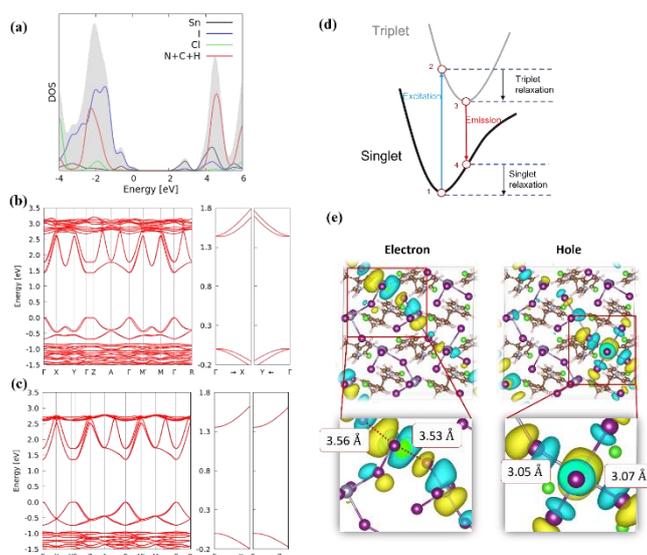
Figure 3. (a) Projected density of states (HSE06-SOC level) of *R*-isomer. Band structure (PBE-SOC level) of (b) *S*- and (c) Racemic isomers. Right panel of the (b) and (c) represents the zoomed figure considering the

four frontier bands. The VBM has been set to zero in both the band structure and DOS figures. The z- and y-direction represent the stacking direction for the chiral and Racemic isomers, respectively. (d) Schematic Jablonski diagram describing the formation mechanism of STEs and the red-shifted PL emission from the STE to the ground state potential energy surface. (e) Kohn-Sham (KS) orbitals of the electron and hole in triplet state.

Table 2. Calculated spin splitting and Rashba parameter for the R- and S-isomers at the frontier valence and conduction bands in various directions.

		CBM				VBM			
		$\Gamma \rightarrow X$	$\Gamma \rightarrow Y$	$\Gamma \rightarrow M'$	$\Gamma \rightarrow M$	$\Gamma \rightarrow X$	$\Gamma \rightarrow Y$	$\Gamma \rightarrow M'$	$\Gamma \rightarrow M$
Splitting Energy (meV)	R	17.8	11.1	11.1	17.8	10.4	16.3	16.4	10.2
	S	16.8	11.0	11.0	16.9	6.8	18.6	18.7	6.68
Rashba Parameter (α)	R	1.06	0.83	0.74	0.99	0.68	0.86	0.77	0.63
	S	1.03	0.82	0.73	0.96	0.55	0.92	0.82	0.51

The computational results confirm the ability of the ClMBA chiral ligands to induce a band splitting which correlates to the emergence of chiroptical properties. Based on the present evidence, the origin of such an effect can be related to the symmetry-breaking distortions in the inorganic layers associated with the ligands. For (R/S-ClMBA)$_2$SnI$_4$, this occurs at the level of the average structure and not to possible local asymmetry within the inorganic framework. Indeed, Mitzi and co-workers highlighted the role of structural descriptor in 2D hybrid perovskites suggesting that spin-splitting could be related to a specific in-plane component of the disparity in adjacent M-X-M bond angles, namely the distortion level of the inter-octahedral bond angles (defined as ($\Delta\beta_{in}$).[43] Such parameter scales linearly with the effective α value (calculated from DFT) for a series of chiral and achiral 2D perovskites.

Interestingly, this correlation does not hold for the present chiral 2D perovskites where the $\Delta\beta_{in}$ parameter is even greater for the racemic sample (not presenting any spin-splitting). It should be noted, however, that the model proposed in ref. 43 refers only to lead-based 2D perovskites. The present results, being the first where the Rashba parameter has been calculated for a Sn-containing 2D chiral perovskite, further point out the strong need to further widen the number and type of chiral

perovskites available. Many open questions still hold, such as the role of spin-orbit coupling related to the nature of the metal ion, the role of local and average inversion symmetry breaking on the emergence of Rashba splitting, the influence of hydrogen bonding, etc. The present paper, while reporting novel chiral lead-free perovskites with one of the lowest band gaps to date, has also highlighted the strong need for further materials chemistry efforts in order to provide solid and reliable structure-property correlations in these appealing materials to pave the way for an effective materials design.

Conclusions

Herein we reported novel lead-free 2D chiral perovskites, namely (R/S-ClMBA)$_2$SnI$_4$. The crystal structure investigation confirmed the crystallization in non-centrosymmetric space groups for the R- and S- enantiomers, opposite to the racemic compound. The presence of chiral ligands effectively induces the emergence of chiroptical properties, as demonstrated by the CD spectra. The optical properties determination by UV-vis spectroscopy and PL shows a direct band gap of about 2.12 eV for the two chiral perovskites and 2.08 for the racemic compound with a broad emission centered around 1.70 eV. DFT calculation confirms Rashba band splitting, with the highest spin splitting values of 17.8 and 18.7 meV for the R- and S-isomer, respectively, and without any splitting for the racemic composition, thus confirming the structural distortion induced by chiral organic cations. Such structural distortions eventually lead to the formation of STEs and concomitant red-shifted emission. Thanks to the reported data on this new system, some preliminary attempts to correlate chiroptical properties to structural distortions and the nature of the central metal are proposed.

Overall, this work reported a novel low band gap Sn-based 2D chiral perovskite which allowed tuning the chiroptical properties through the inclusion of Cl-MBA ligand and provided novel clues to extend the actual comprehension of the structure-property correlations in chiral perovskites.

Supporting Information

The authors have cited additional references within the Supporting Information.[44-59]

Acknowledgements

Keywords: metal halide perovskites • chiral perovskites • computational modelling • lead-free perovskites • chiroptoelectronics

[1] Y. Dang, X. Liu, B. Cao, X. Tao, *Matter* **2021**, *4*, 794–820.

[2] G. Long, R. Sabatini, M. I. Saidaminov, G. Lakhwani, A. Rasmita, X. Liu, E. H. Sargent, W. Gao, *Nat Rev Mater* **2020**, *5*, 423–439.

[3] Y. Dong, Y. Zhang, X. Li, Y. Feng, H. Zhang, J. Xu, *Small* **2019**, *15*, 1902237.

[4] J. Ma, H. Wang, D. Li, *Adv. Mater.* **2021**, *33*, 2008785.

[5] D. G. Billing, A. Lemmerer, *CrystEngComm* **2006**, *8*, 686–695.

[6] J. Ma, C. Fang, C. Chen, L. Jin, J. Wang, S. Wang, J. Tang, D. Li, *ACS Nano* **2019**, *13*, 3659–3665.

[7] C. Yang, W. Chen, Y. Ding, J. Wang, Y. Rao, W. Liao, Y. Tang, P. Li, Z. Wang, R. Xiong, *Adv. Mater.* **2019**, *31*, 1808088.

[8] M. K. Jana, R. Song, H. Liu, D. R. Khanal, S. M. Janke, R. Zhao, C. Liu, Z. Valy Vardeny, V. Blum, D. B. Mitzi, *Nat Commun* **2020**, *11*, 4699.

[9] T. Liu, W. Shi, W. Tang, Z. Liu, B. C. Schroeder, O. Fenwick, M. J. Fuchter, *ACS Nano* **2022**, *16*, 2682–2689.

[10] G. Long, C. Jiang, R. Sabatini, Z. Yang, M. Wei, L. N. Quan, Q. Liang, A. Rasmita, M. Askerka, G. Walters, X. Gong, J. Xing, X. Wen, R. Quintero-Bermudez, H. Yuan, G. Xing, X. R. Wang, D. Song, O. Voznyy, M. Zhang, S. Hoogland, W. Gao, Q. Xiong, E. H. Sargent, *Nature Photon* **2018**, *12*, 528–533.

[11] Y. Peng, Y. Yao, L. Li, Z. Wu, S. Wang, J. Luo, *J. Mater. Chem. C* **2018**, *6*, 6033–6037.

[12] C. Yuan, X. Li, S. Semin, Y. Feng, T. Rasing, J. Xu, *Nano Lett.* **2018**, *18*, 5411–5417.

[13]   C. Chen, L. Gao, W. Gao, C. Ge, X. Du, Z. Li, Y. Yang, G. Niu, J. Tang, *Nat Commun* **2019**, *10*, 1927.

[14]   J. Ahn, S. Ma, J.-Y. Kim, J. Kyhm, W. Yang, J. A. Lim, N. A. Kotov, J. Moon, *J. Am. Chem. Soc.* **2020**, *142*, 4206–4212.

[15]   D. Fu, J. Xin, Y. He, S. Wu, X. Zhang, X. Zhang, J. Luo, *Angew Chem Int Ed* **2021**, *60*, 20021–20026.

[16]   Y. Dang, X. Liu, Y. Sun, J. Song, W. Hu, X. Tao, *J. Phys. Chem. Lett.* **2020**, *11*, 1689–1696.

[17]   H. Lu, J. Wang, C. Xiao, X. Pan, X. Chen, R. Brunecky, J. J. Berry, K. Zhu, M. C. Beard, Z. V. Vardeny, *Sci. Adv.* **2019**, *5*, eaay0571.

[18]   J. Ahn, E. Lee, J. Tan, W. Yang, B. Kim, J. Moon, *Mater. Horiz.* **2017**, *4*, 851–856.

[19]   G. Long, Y. Zhou, M. Zhang, R. Sabatini, A. Rasmita, L. Huang, G. Lakhwani, W. Gao, *Adv. Mater.* **2019**, *31*, 1807628.

[20]   Z. Guo, J. Li, C. Wang, R. Liu, J. Liang, Y. Gao, J. Cheng, W. Zhang, X. Zhu, R. Pan, T. He, *Angew. Chem. Int. Ed.* **2021**, *60*, 8441–8445.

[21]   J. Hao, H. Lu, L. Mao, X. Chen, M. C. Beard, J. L. Blackburn, *ACS Nano* **2021**, *15*, 7608–7617.

[22]   B. Li, Y. Yu, M. Xin, J. Xu, T. Zhao, H. Kang, G. Xing, P. Zhao, T. Zhang, S. Jiang, *Nanoscale* **2023**, *15*, 1595–1601.

[23]   Y. Lu, Q. Wang, R. He, F. Zhou, X. Yang, D. Wang, H. Cao, W. He, F. Pan, Z. Yang, C. Song, *Angew. Chem. Int. Ed.* **2021**, *60*, 23578–23583.

[24]   R. Das, M. Hossain, A. Mahata, D. Swain, F. De Angelis, P. K. Santra, D. D. Sarma, *ACS Materials Lett.* **2023**, 1556–1564.

[25]   H. Lu, C. Xiao, R. Song, T. Li, A. E. Maughan, A. Levin, R. Brunecky, J. J. Berry, D. B. Mitzi, V. Blum, M. C. Beard, *J. Am. Chem. Soc.* **2020**, *142*, 13030–13040.

[26]   M. Konstantakou, T. Stergiopoulos, *J. Mater. Chem. A* **2017**, *5*, 11518–11549.

[27]   J. Cao, F. Yan, *Energy Environ. Sci.* **2021**, *14*, 1286–1325.

[28]   M. Pitaro, E. K. Tekelenburg, S. Shao, M. A. Loi, *Advanced Materials* **2022**, *34*, 2105844.

[29]   R. Chiara, M. Morana, G. Folpini, A. Olivati, B. Albini, P. Galinetto, L. Chelazzi, S. Ciattini, E. Fantechi, S. A. Serapian, A. Petrozza, L. Malavasi, *J. Mater. Chem. C* **2022**, *10*, 12367–12376.

[30]   R. Chiara, M. Morana, M. Boiocchi, M. Coduri, M. Striccoli, F. Fracassi, A. Listorti, A. Mahata, P. Quadrelli, M. Gaboardi, C. Milanese, L. Bindi, F. De Angelis, L. Malavasi, *J. Mater. Chem. C* **2021**, *9*, 9899–9906.

[31]   K. Robinson, G. V. Gibbs, P. H. Ribbe, *Science* **1971**, *172*, 567–570.

[32]   W. H. Baur, *Acta Crystallogr B Struct Sci* **1974**, *30*, 1195–1215.

[33]   A. Ben-Moshe, A. Teitelboim, D. Oron, G. Markovich, *Nano Lett.* **2016**, *16*, 7467–7473.

[34]   J. Lin, D. Chen, L. Yang, T. Lin, Y. Liu, Y. Chao, P. Chou, C. Chiu, *Angew Chem Int Ed* **2021**, *60*, 21434–21440.

[35]   X. Li, J. M. Hoffman, M. G. Kanatzidis, *Chem. Rev.* **2021**, *121*, 2230–2291.

[36]   D. Cortecchia, J. Yin, A. Petrozza, C. Soci, *J. Mater. Chem. C* **2019**, *7*, 4956–4969.

[37]   D. Cortecchia, S. Neutzner, A. R. Srimath Kandada, E. Mosconi, D. Meggiolaro, F. De Angelis, C. Soci, A. Petrozza, *J. Am. Chem. Soc.* **2017**, *139*, 39–42.

[38]   T. Etienne, E. Mosconi, F. De Angelis, *J. Phys. Chem. Lett.* **2016**, *7*, 1638–1645.

[39]   Abd. R. B. Mohd Yusoff, A. Mahata, M. Vasilopoulou, H. Ullah, B. Hu, W. Jose Da Silva, F. Kurt Schneider, P. Gao, A. V. Ievlev, Y. Liu, O. S. Ovchinnikova, F. De Angelis, M. Khaja Nazeeruddin, *Materials Today* **2021**, *46*, 18–27.

[40]   A. Bernasconi, A. Rizzo, A. Listorti, A. Mahata, E. Mosconi, F. De Angelis, L. Malavasi, *Chem. Mater.* **2019**, *31*, 3527–3533.

[41]   L. Malavasi, W. Kaiser, F. De Angelis, E. Mosconi, M. Morana, R. Chiara, D. Meggiolaro, P. Galinetto, B. Albini, *Origin of Broad Emission Induced by Rigid Aromatic Ditopic Cations in Low-Dimensional Metal Halide Perovskites*, Chemistry, **2023**.

[42]   S. Kahmann, D. Meggiolaro, L. Gregori, E. K. Tekelenburg, M. Pitaro, S. D. Stranks, F. De Angelis, M. A. Loi, *ACS Energy Lett.* **2022**, *7*, 4232–4241.

[43]   M. K. Jana, R. Song, Y. Xie, R. Zhao, P. C. Sercel, V. Blum, D. B. Mitzi, *Nat Commun* **2021**, *12*, 4982.